Electron Microscopy

DOI: 10.1002/anie.201301236

# Direct Atomic-Resolution Observation of Two Phases in the $Li_{1.2}Mn_{0.567}Ni_{0.166}Co_{0.067}O_2$ Cathode Material for Lithium-Ion Batteries**

*Haijun Yu, Ryo Ishikawa, Yeong-Gi So, Naoya Shibata, Tetsuichi Kudo, Haoshen Zhou,* and Yuichi Ikuhara**

The Lithium–manganese-rich layered oxides (LLOs, $Li_{1+x}Mn_yTM_{1-x-y}O_2$, TM = Ni, Co, Mn, Fe, or Cr) are the most attractive cathode materials for lithium-ion batteries, because of their high discharge capacities (ca. 280 mA h g$^{-1}$), and energy density (ca. 1000 Wh kg$^{-1}$; Figure 1a). These values are two times larger than those of conventional cathode materials of lithium-ion batteries.[1] However, the structures of these materials are still ambiguous and the subject of ongoing debate.

It has been proposed that these LLOs are composed of two phases, one rhombohedral $LiTMO_2$ phase (space group: $R\bar{3}m$; TM = Ni, Co, Mn, Fe, and Cr), and the other monoclinic $Li_2MnO_3$-like phase (space group: $C2m$), shown in Figure 1b and Figure 1c, respectively.[1f,2] The large rechargeable capacities mainly arise from the activation of $Li_2MnO_3$-like phases inside LLOs when the Li/LLOs cells are electrochemically charged to over 4.4 V during the 1st cycle.[1f,2a,3] Furthermore, based on this proposition, the charge/discharge curves and redox reactions during the 1st and following cycles of these LLOs at room temperature can be explained well.[1f,2a,b] However, although the synchrotron X-ray diffraction (SXRD),[2a] nuclear magnetic resonance (NMR),[2c,4] extended X-ray absorption fine structure (EXAFS)[2c,e] spectroscopy, and high-resolution transmission electron microscopy (HRTEM)[2d–h] results have suggested that the two phases are present inside these LLOs, there is still no strong evidence, such as the direct observation of intergrowth two-phase in one crystalline grain because of their similar interlayer spacing (ca. 4.7 Å) along $[001]_{rh}$ and $[103]_{mon}$ directions (the subscripts of "rh" and "mon" stand for the Bravais lattices of rhombohedral and monoclinic, respectively). Thus, some researchers think that these LLOs should form a homogeneous solid solution between the $Li_2MnO_3$ and $LiTMO_2$ component.[5] Until now, there has been much debate on the average/local structure of these LLOs and how they related to the electrochemical properties.[1f,2c,e,4–6] Direct imaging of the intergrowth two-phase and hetero-interface at the atomic scale is essential to clarify the debate, and to full understand and precisely control the electrochemical properties of these LLOs.

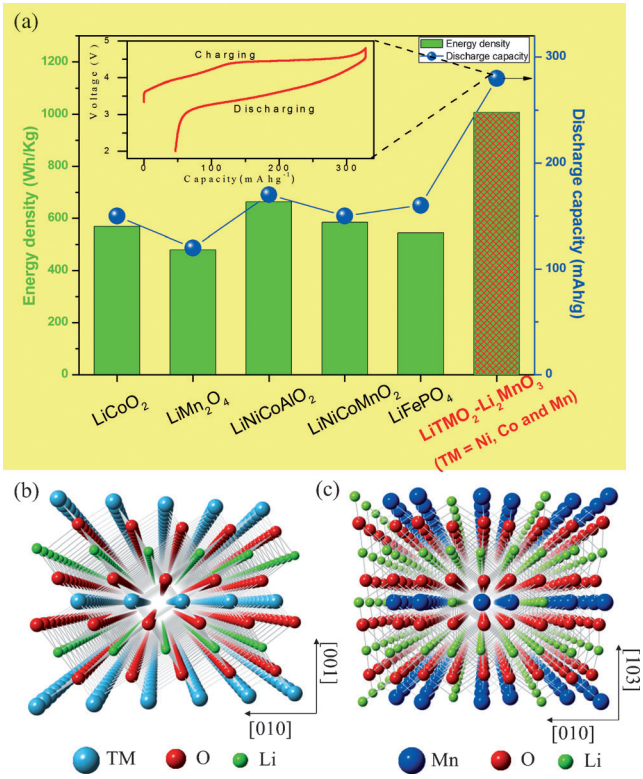


***Figure 1.*** a) Energy density and rechargeable capacity of the main cathode materials for lithium-ion batteries. b) Crystal structure of the rhombohedral $LiTMO_2$ structure (space group: $R\bar{3}m$, TM = Ni, Co, and Mn) and c) monoclinic $Li_2MnO_3$-like structure (space group: $C2m$) viewed from the [100] crystallographic direction.

[*] Dr. H. J. Yu,[+] Prof. T. Kudo, Prof. H. S. Zhou
Energy Technology Research Institute, National Institute of Advanced Industrial Science and Technology (AIST)
Umezono 1-1-1, Tsukuba, 305-8568 (Japan)
E-mail: hs.zhou@aist.go.jp
Dr. R. Ishikawa,[+] Dr. Y. G. So, Dr. N. Shibata, Prof. Y. Ikuhara
Institute of Engineering Innovation, The University of Tokyo
Tokyo, 113-8654 (Japan)
E-mail: ikuhara@sigma.t.u-tokyo.ac.jp
Prof. T. Kudo
Department of Applied Chemistry, The University of Tokyo
Tokyo, 113-8656 (Japan)
Prof. H. S. Zhou
Department of Chemical System Engineering, The University of Tokyo
Tokyo, 113-8656 (Japan)
[+] These authors contributed equally to this work.
[**] This work was partially supported financially by the Funding Program for World-Leading Innovative R&D on Science and Technology (FIRST Program).
Supporting information for this article is available on the WWW under http://dx.doi.org/10.1002/anie.201301236.

Herein we show the direct observation of the intergrowth of an $Li_2MnO_3$-like structure with a bulk $LiTMO_2$ structure and hetero-interface in grains of the $Li_{1.2}Mn_{0.567}Ni_{0.166}Co_{0.067}O_2$ Lithium–manganese-rich layered oxide material (Supporting Information, Figure S1) by using atomic-resolution scanning transmission electron microscopy (STEM). To determine the atomic structure of the two phases, the newly developed annular bright-field (ABF)[7] STEM in combination with high-angle annular dark-field (HAADF) STEM techniques are introduced to reveal the LLOs for the first time. We can definitely image not only oxygen atoms but also the ultra-light lithium atoms, and thus we can image all the chemical types present and directly determine the local structure of the two phases and the hetero-interface. Thus, the strong evidence for rhombohedral $LiTMO_2$ (TM = Ni, Co, and Mn) and monoclinic $Li_2MnO_3$-like phases coexisting in the studied LLO material are presented at atomic resolution. Furthermore, the hetero-interface along the $[001]_{rh}/[103]_{mon}$ zone axis direction of the intergrowth two-phase domains is clearly revealed. These results demonstrate the two-phase nature rather than a homogenous solid solution, and are consistent with the proposed electrochemical reaction mechanism of these LLOs.[1f]

The structure of the LLO was investigated by selected-area electron diffraction (SAED), and we found two types of phases: $LiTMO_2$ and $Li_2MnO_3$-like phases. The results are consistent with our previous average structure study by SXRD on this LLO.[2a] Figure 2a shows a typical SAED pattern obtained from the $LiTMO_2$ phase along the $[100]_{rh}$ crystallographic direction and the $Li_2MnO_3$-like phase along the $[010]_{mon}$ crystallographic direction, respectively, which is reproduced by the simulation, shown in Figure 2d and Figure S2. The SAED patterns, shown in Figure 2b and c, can also be interpreted as the two-phase coexistence of $LiTMO_2$ and $Li_2MnO_3$-like phases along the different zone axes. Figure 2b contains not only $\bar{1}\bar{1}3n$ ($n$ is integer) reflections for $LiTMO_2$ structure but also additional spotted-streaks along the $c^*$-axis. These spotted-streaks are consistent with ordering of the Li in the $LiMn_2$-like planes and are the signature of platelets with an $Li_2MnO_3$-like phase normal to the $[001]_{rh}$ zone axis. The experimental SAED patterns in Figure 2b can be reproduced well by the simulation in Figure 2e. It is clear that the SAED patterns of $LiTMO_2$ structure viewed along the $[0\bar{1}0]_{rh}$ orientation and of $Li_2MnO_3$-like structure viewed along the $[1\bar{1}0]_{mon}$, $[100]_{mon}$ and $[110]_{mon}$ orientations are overlapping (see Figure S3-A). The different reflections planes inside the $Li_2MnO_3$-like structural unit suggest that there is a high density of stacking faults in this LLO, the streaks in Figure 2b result from these stacking faults with thin platelets along the $[001]_{rh}$ orientation, while the sharp spots are indicative of thicker platelets.

Figure 2c shows the SAED patterns viewed along the $[001]_{rh}$ direction. The highlighted dashed hexagon shows the overall hexagonal symmetry of the SAED patterns, while the dashed parallelogram shows the unit cell of the $LiTMO_2$ structural unit. Figure 2c can be well reproduced using the SAED simulation in Figure 2f, it is clear that $\bar{1}\bar{1}0_{rh}$, $1\bar{2}0_{rh}$, and $2\bar{1}0_{rh}$ reflections originated from the $LiTMO_2$ structure are completely superposed with the reflections originating from the $Li_2MnO_3$-like structure, while the additional super-reflections occurring inside and on the edges of the rhombohedral unit cell originate from the reflections of $Li_2MnO_3$-like structural unit (see Figure S3-B). The SAED patterns combined with the simulations or SXRD patterns tell us the possibility of two-phase existence in the present LLO, however it is still difficult to reveal the local configurations of the two phases at the atomic scale. Figure 3a and b show the simultaneously recorded HAADF and ABF STEM images obtained from the $LiTMO_2$ domains in the present LLO. These images are consistent with the $LiTMO_2$ structure projected along the $[100]_{rh}$ direction (see Figure S4). The bright-dot contrast in HAADF STEM images (Figure 3a) and dark-dot contrast in ABF STEM images (Figure 3b)

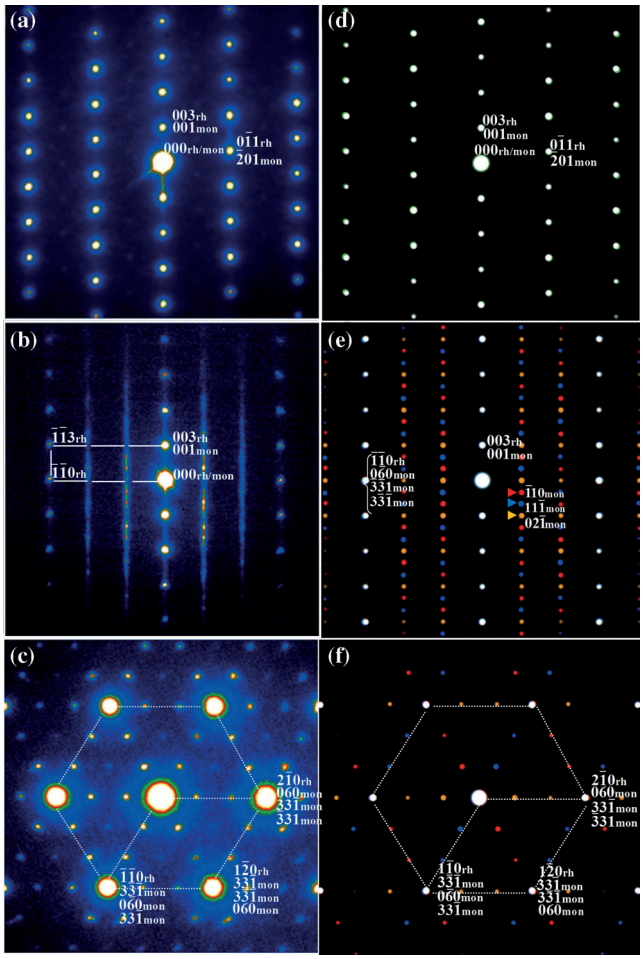


***Figure 2.*** a) Overlapping SAED patterns of the $LiTMO_2$ structure reflection projected along $[100]_{rh}$ direction and of the $Li_2MnO_3$-like structural units reflection projected along $[010]_{mon}$. b) Overlapping SAED patterns of the $LiTMO_2$ structure reflection projected along $[1\bar{1}0]_{rh}$ direction and of the $Li_2MnO_3$-like structural units reflection projected along $[1\bar{1}0]_{mon}$, $[100]_{mon}$ and $[110]_{mon}$ directions. c) Overlapping SAED patterns of the $LiTMO_2$ structural and $Li_2MnO_3$-like structure unit reflection projected along $[001]_{rh}/[103]_{mon}$ direction. d), e), and f) Simulated SAED patterns corresponding to experimental SAED in (a),(b), and (c). The white reflection patterns in (d)–(f) show the simulated SAED patterns reflected from the $LiTMO_2$ structural unit, while the different green, red, yellow, and blue reflection patterns indicate the different reflected planes in the $Li_2MnO_3$-like structural unit.

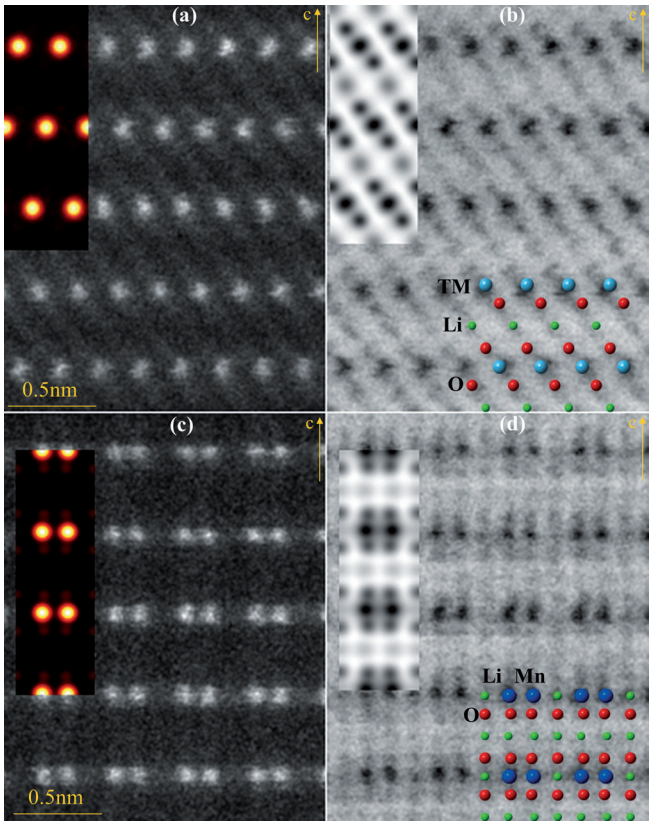


***Figure 3.*** a) and b) HAADF and ABF STEM images of the rhombohedral $LiTMO_2$ structure projected along the $[100]_{rh}$ direction. c) and d) HAADF and ABF STEM images of the monoclinic $Li_2MnO_3$-like structure projected along the $[100]_{mon}$ direction. Insets: (top left) simulated HAADF and ABF STEM images of the rhombohedral $LiTMO_2$ and monoclinic $Li_2MnO_3$-like structures based on fast-Fourier-transform multislice algorithm. Insets: (bottom right) of (b) and (d) are the crystal-structure image of the rhombohedral $LiTMO_2$ and monoclinic $Li_2MnO_3$-like structures, respectively.

show the transitional-metal (TM) atom column positions, the faint but distinct dark-dot contrast in the interlayer positions of ABF STEM image (Figure 3b) can be recognized as the lithium and oxygen-atom column positions in the $LiTMO_2$ structure. The simulated images on $LiTMO_2$ structure, inserted in each experimental image, reproduce fairly well all the observed features.

In addition to $LiTMO_2$ structure, we found $Li_2MnO_3$-like structure domains in the same grain. Figure 3c and 3d show atomic-resolution HAADF and ABF STEM images of monoclinic $Li_2MnO_3$-like structure, projected along the $[100]_{mon}$ orientation (see Figure S5) to the *c*-axis. In HAADF STEM image, only Mn atoms (or other TM metals) are visualized as bright spots, corresponding to the $LiMn_2$-like layer features. While in the ABF STEM image, we can observe not only TM atoms but also oxygen (next to the $LiMn_2$-like layer) and even lithium atoms (between oxygen layers or between Mn atoms within $LiMn_2$-like layers) as dark dot contrasts. The observed features in Figure 3c and d are well reproduced by the image simulation (see insets), suggesting that $LiTMO_2$ and $Li_2MnO_3$-like structures are coexisting in the same grain. Our experimental results directly demonstrate the two-phase coexistence of $LiTMO_2$ and $Li_2MnO_3$-like structures. However, there are still some important issues that need to be clarified: in particular the local atomic structure of the hetero-interface between the two phases.

Figure 4a shows the atomic-resolution HAADF STEM image obtained from the hetero-interface between $LiTMO_2$ and $Li_2MnO_3$-like structures. There are two individual domain regions marked by the blue dashed-line rectangles. In the region I, there are four horizontal bright bands corresponding to the TM planes of the LLO. In the 1st, 2nd, and 4th bright bands, each row consists of a periodic sequence of two bright spots and a dark spot, corresponding to the $LiMn_2$-like layers of the $Li_2MnO_3$-like structural units. While, in the 3rd bright band (between the 2nd and 4th bright band), the bright spots are aligned to form continuous lattice fringes with 0.14 nm inter-column spacing, and are associated with the $LiTMO_2$ structural unit projected along the $[1\bar{1}0]_{rh}$ direction. Until now, evidence for two-phase coexistence is similar to the phenomenon of region I in Figure 4a.[2d,g] While in region II of Figure 4a, two arrangements of bright spots are presented and separated into two different domains: sequences of two bright spots and a dark spot are shown in the 5th, 6th, and 7th bright bands, and continuous bright spots are shown in the 8th, 9th, and 10th bright bands.

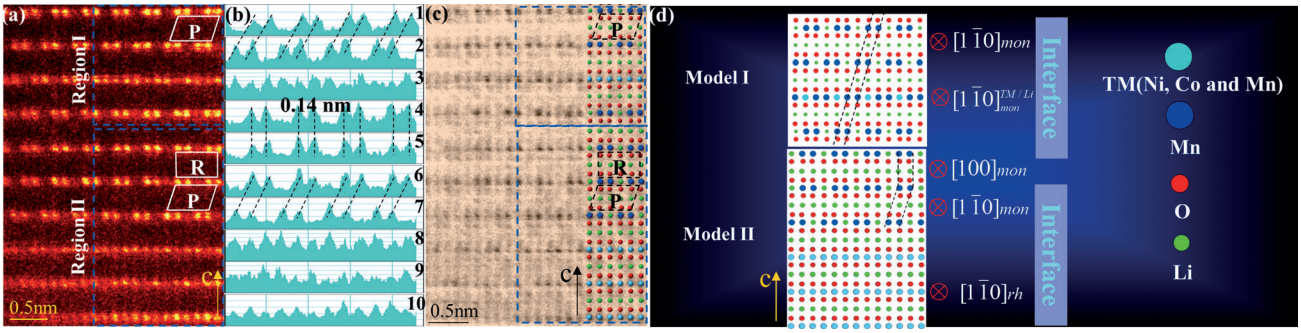


***Figure 4.*** a) HAADF and c) ABF-STEM images of the intergrowth two-phase and hetero-interface in the same local region along the $[001]_{rh}$ zone axis direction. b) Intensity profiles of each bright band (1–10) inside the two regions in (a) along horizontal direction. d) Two proposed interface models based on (c). The inserted parallelogram and rectangle in (a) show the different parallelogram and rectangular symmetry of the monoclinic $Li_2MnO_3$-like structure. Inserted image in (c) shows the whole intergrowth two-phase and hetero-interface atomic arrangements inside the LLO.

The 5th, 6th, and 7th rows are associated with the local monoclinic ordering of the $LiMn_2$-like layer present in the TM planes, while 8th, 9th, and 10th rows are consistent with local rhombohedral ordering of the TM–TM atom arrangement in the TM planes. The region II gives strong evidence for the two-phase coexistence of $LiTMO_2$ and $Li_2MnO_3$-like structures, and is also in agreement with the former discussion of the SAED patterns and HAADF/ABF STEM images. The intensity profiles along the ten bright bands in Figure 4a are shown in Figure 4b, showing the periodicity of the inter-column spacing of the regions I and II, and revealing the two-phases of the $LiTMO_2$ and $Li_2MnO_3$-like structures can coexist inside the LLO. Furthermore, the ABF STEM image of the intergrowth and hetero-interface with visible lithium and oxygen atomic columns in the same region of the LLO is shown in Figure 4c, and the validity of relative atomic positions is demonstrated clearly by the inserted crystal-structure image model.

On the basis of the atomic arrangement of the intergrowth and hetero-interface inside the single LLO grain, two interface models can be proposed and are shown in Figure 4d. In the model I, we consider that there is a single plane of the $LiTMO_2$ structural unit oriented along the $[1\bar{1}0]_{rh}$ direction inside the $Li_2MnO_3$-like structure oriented along the $[1\bar{1}0]_{mon}$ direction. We can also suppose that a few Li atomic sites in the $LiMn_2$-like layer of the $Li_2MnO_3$-like structural units orientated along the $[1\bar{1}0]_{mon}$ direction are occupied by TM atoms, which can be notated as $[1\bar{1}0]_{mon}^{TM/Li}$. Model I is ambiguous on distinguishing the two-phase coexistence. While, in the model II, the large domains with the $LiTMO_2$ structural unit orientated along the $[1\bar{1}0]_{rh}$ direction and with the $Li_2MnO_3$-like structural unit orientated along the $[100]_{mon}$ and $[1\bar{1}0]_{mon}$ directions integrate together along the *c*-axis, and the hetero-interfaces of these two structural units are presented along the $[001]_{rh}/[103]_{mon}$ orientation.

The lithium ion in the transitional-metal layer of this LLO (0.2 in $Li[Li_{0.2}Mn_{0.567}Ni_{0.166}Co_{0.067}]O_2$) is not enough to support the overall Li-TM-TM (Li:TM = 2) periodic ordering compared with that of $Li_2MnO_3$ (0.33 in $Li[Li_{0.33}Mn_{0.67}]O_2$). Thus, coexistence of the two structures associated with TM-TM and Li-TM-TM periodic ordering in the transitional-metal layer is the most probable outcome. In addition, the parallelogram and rectangle symmetry (the inserted white boxes in Figure 4a, the black dashed line in Figure 4c and d) observed inside the LLO give direct evidence that a high density of stacking faults exists inside the $Li_2MnO_3$-like structure, which is consistent with the SAED pattern analysis.

In conclusion, electron diffraction and state-of-the-art ABF/HAADF STEM imaging combined with computer simulations provide direct access to the local atomic arrangement of the $Li_{1.2}Mn_{0.567}Ni_{0.166}Co_{0.067}O_2$ lithium-rich layered oxide material for lithium-ion batteries. The intergrowth of rhombohedral $LiTMO_2$ (TM = Ni, Co, and Mn)/monoclinic $Li_2MnO_3$-like structures and their hetero-interfaces inside this material are directly revealed at the atomic scale. The domains with these two structures are separated by the $(001)_{rh}/(103)_{mon}$ plane along the $[001]_{rh}/[103]_{mon}$ orientation, strongly supporting the local structure variation of these LLOs. Ongoing efforts are focused on the local component analysis by energy dispersive spectrometry (EDS) and local structure variation influenced by different charge/discharge states.

## Experimental Section

The $Li_{1.2}Mn_{0.567}Ni_{0.166}Co_{0.067}O_2$ lithium-rich layered oxide materials are prepared by a solid-state reaction method, and the detailed synthesis process and characterization with synchrotron X-ray diffraction and X-ray diffraction are shown in Ref. [2a,b]. The thin specimens for TEM or STEM observations were prepared by softly crushing fine particles in ethanol and dispersing it onto perforated amorphous carbon films. SAED patterns and BF-TEM images were taken with a 200 kV JEM-2010HC electron microscope (JEOL), and the possible overlapping SAED figures are calculated. Atomic-resolution ABF/HAADF-STEM images were taken with a 200 kV ARM-200CF electron microscope (JEOL) equipped with an aberration corrector and a cold field-emission gun. The microscope conditions for the atomic-scale analysis are: the probe-forming aperture half-angle is 24.5 mrad and half-angles of the ABF and HAADF detectors are 12–24.5 mrad and 68–280 mrad, respectively. The HAADF/ABF-STEM image simulations were carried out by the xHREM software (HREM research Inc.).

Received: February 12, 2013
Published online: April 24, 2013

**Keywords:** cathode materials · electron microscopy · hetero-interfaces · layered oxides · lithium-ion battery

[1] a) J. M. Tarascon, M. Armand, *Nature* **2008**, *451*, 652–657; b) A. S. Aricò, P. Bruce, B. Scrosati, J. M. Tarascon, W. Van Schalkwijk, *Nat. Mater.* **2005**, *4*, 366–377; c) S. H. Kang, P. Kempgens, S. Greenbaum, A. J. Kropf, K. Amine, M. M. Thackeray, *J. Mater. Chem.* **2007**, *17*, 2069–2077; d) P. He, H. J. Yu, D. Li, H. S. Zhou, *J. Mater. Chem.* **2012**, *22*, 3680–3695; e) H. J. Yu, H. S. Zhou, *J. Mater. Chem.* **2012**, *22*, 15507–15510; f) M. M. Thackeray, S. H. Kang, C. S. Johnson, J. T. Vaughey, R. Benedek, S. A. Hackney, *J. Mater. Chem.* **2007**, *17*, 3112–3125.

[2] a) H. J. Yu, H. J. Kim, Y. R. Wang, P. He, D. Asakura, Y. Nakamura, H. S. Zhou, *Phys. Chem. Chem. Phys.* **2012**, *14*, 6584–6595; b) H. J. Yu, Y. R. Wang, D. Asakura, E. Hosono, H. S. Zhou, *RSC Adv.* **2012**, *2*, 8797–8807; c) W. S. Yoon, N. Kim, X. Q. Yang, J. McBreen, C. P. Grey, *J. Power Sources* **2003**, *119*, 649–653; d) J. Bareño, M. Balasubramanian, S. H. Kang, J. G. Wen, C. H. Lei, S. V. Pol, I. Petrov, D. P. Abraham, *Chem. Mater.* **2011**, *23*, 2039–2050; e) J. Bareño, C. H. Lei, J. G. Wen, S. H. Kang, I. Petrov, D. P. Abraham, *Adv. Mater.* **2010**, *22*, 1122–1127; f) A. Boulineau, L. Simonin, J. F. Colin, E. Canevet, L. Daniel, S. Patoux, *Chem. Mater.* **2012**, *24*, 3558–3566; g) J. G. Wen, J. Bareno, C. H. Lei, S. H. Kang, M. Balasubramanian, I. Petrov, D. P. Abraham, *Solid State Ionics* **2011**, *182*, 98–107; h) J. Kikkawa, T. Akita, M. Tabuchi, M. Shikano, K. Tatsumi, M. Kohyama, *J. Appl. Phys.* **2008**, *103*, 104911.

[3] A. R. Armstrong, M. Holzapfel, P. Novak, C. S. Johnson, S. H. Kang, M. M. Thackeray, P. G. Bruce, *J. Am. Chem. Soc.* **2006**, *128*, 8694–8698.

[4] C. J. Pan, Y. J. Lee, B. Ammundsen, C. P. Grey, *Chem. Mater.* **2002**, *14*, 2289–2299.

[5] K. A. Jarvis, Z. Q. Deng, L. F. Allard, A. Manthiram, P. J. Ferreira, *Chem. Mater.* **2011**, *23*, 3614–3621.

[6] T. Ohzuku, M. Nagayama, K. Tsuji, K. Ariyoshi, *J. Mater. Chem.* **2011**, *21*, 10179–10188.

[7] a) S. D. Findlay, N. Shibata, H. Sawada, E. Okunishi, Y. Kondo, T. Yamamoto, Y. Ikuhara, *Appl. Phys. Lett.* **2009**, *95*, 191913; b) N.

  

Shibata, M. F. Chisholm, A. Nakamura, S. J. Pennycook, T. Yamamoto, Y. Ikuhara, *Science* **2007**, *316*, 82 – 85; c) Y. Ishikawa, H. Nagayama, H. Hoshino, M. Ohgai, N. Shibata, T. Yamamoto, Y. Ikuhara, *Mater. Trans.* **2009**, *50*, 959 – 963; d) L. Gu, C. B. Zhu, H. Li, Y. Yu, C. L. Li, S. Tsukimoto, J. Maier, Y. Ikuhara, *J. Am. Chem. Soc.* **2011**, *133*, 4661 – 4663; e) R. Huang, Y. H. Ikuhara, T. Mizoguchi, S. D. Findlay, A. Kuwabara, C. A. J. Fisher, H. Moriwake, H. Oki, T. Hirayama, Y. Ikuhara, *Angew. Chem.* **2011**, *123*, 3109 – 3113; *Angew. Chem. Int. Ed.* **2011**, *50*, 3053 – 3057; f) Z. C. Wang, W. Zeng, L. Gu, M. Saito, S. Tsukimoto, Y. Ikuhara, *J. Appl. Phys.* **2010**, *108*, 113701-113709; g) X. Lu, Z. L. Jian, Z. Fang, L. Gu, Y. S. Hu, W. Chen, Z. X. Wang, L. Q. Chen, *Energy Environ. Sci.* **2011**, *4*, 2638 – 2644; h) L. M. Suo, W. Z. Han, X. Lu, L. Gu, Y. S. Hu, H. Li, D. F. Chen, L. Q. Chen, S. Tsukimoto, Y. Ikuhara, *Phys. Chem. Chem. Phys.* **2012**, *14*, 5363 – 5367; i) X. Lu, L. Zhao, X. Q. He, R. J. Xiao, L. Gu, Y. S. Hu, H. Li, Z. X. Wang, X. F. Duan, L. Q. Chen, J. Maier, Y. Ikuhara, *Adv. Mater.* **2012**, *24*, 3233 – 3238; j) X. Lu, Y. Sun, Z. L. Jian, X. Q. He, L. Gu, Y. S. Hu, H. Li, Z. X. Wang, W. Chen, X. F. Duan, L. Q. Chen, J. Maier, S. Tsukimoto, Y. Ikuhara, *Nano Lett.* **2012**, *12*, 6192 – 6197.

  